Materials Research Proceedings 64 (2026) 863-870 https://doi.org/10.21741/9781644904091-107

Field Oriented Control based on Sliding Mode of a Variable Speed Grid-Connected DFIG Wind Turbine System

Aymen BOUJEMEL[1,a *], Najib EL OUANJLI[2,b], Hicham ROUIJAA[1,c], Ayoub NOUAITI[2,d], Ilias EN-NAOUI[1,e], and Mostafa MERRAS[3,f],

[1]Energy-Matter-Instrumentation & Telecoms, Faculty of science and technology, Hassan 1st university, Settat, Morocco

[2]LASMAR Laboratory, SEIMC Research Team, Higher School of Technology, Moulay Ismail University, Meknes, Morocco

[3]IMACS Laboratory, Higher School of Technology, Moulay Ismail University, Meknes, Morocco

[a]aymen.boujemel.doc@uhp.ac.ma, [b]n.elouanjli@umi.ac.ma, [c]hrouijaa@gmail.com, [d]a.nouaiti@umi.ac.ma, [e]i.ennaoui@uhp.ac.ma, [f]m.merras@umi.ac.ma

Keywords: Variable-Speed Wind-Turbine System, Tip-Speed Ratio, DFIG, FOC, MPPT, SMC

Abstract. This study introduces a control scheme for wind energy conversion systems based on a doubly fed induction generator (DFIG) that integrates a tip-speed-ratio (TSR)-oriented Maximum Power Point Tracking (MPPT) technique with a direct vector control scheme enhanced by sliding mode control. The proposed method aims to maximize active power extraction under varying wind conditions while ensuring zero reactive power output to support grid stability. The partial-scale converter design inherent to the DFIG configuration offers cost and efficiency advantages, while the adopted control techniques improve dynamic response and reliability. The simulation results reveal that the suggested method significantly ameliorates the system's performance. The MPPT speed control had a rise time of 2.5 ms, while the power control had a rise time of 1.5 ms.

1. Introduction

Wind turbine construction has been widely developed in recent decades due to the renewable energy policy and electricity requirement throughout the world [1]. Most of today's systems are variable speed in nature from which the MPPT and the powers control is achieved through use of power converters [2], [3]. Of the existing technologies, DFIGs are used most, and it is due to their low cost; light weight and good grid support facilities [4].

In a DFIG system, the stator is directly connected to the grid, whereas the rotor is supplied via a bidirectional power converter, allowing variable-speed operation while staying synchronized with the grid voltage and frequency (Fig. 1). The converter compensates slip and ensures stable power generation even at sub-synchronous speeds [5]. A key advantage is the partial-scale converter, which handles only 25–30% of rated power, reducing losses and cost while allowing full regulation of active and reactive power for grid support [6].

The generator control relies on the RSC for torque and power regulation and the GSC for DC bus voltage control [7]. MPPT is used to define electromagnetic torque reference and, therefore, the active power command, in contrast, setting the reactive power command to zero is generally adopted to improve the power factor. Vector control enables the distinct regulation of active and reactive power, by adjusting the rotor speed to maintain the optimal tip-speed ratio through a TSR-based MPPT. In this work, TSR-based MPPT is combined with vector control enhanced by SMC technique to regulate the power flow.

Content from this work may be used under the terms of the Creative Commons Attribution 3.0 license. Any further distribution of this work must maintain attribution to the author(s) and the title of the work, journal citation and DOI. Published under license by Materials Research Forum LLC.

Materials Research Proceedings 64 (2026) 863-870 https://doi.org/10.21741/9781644904091-107

The rest of this article is arranged as follows. The second section details the system modeling, Section 3 introduces the suggested control strategy, Section 4 extends and analyzes the simulation results, and last section provides the final conclusions.

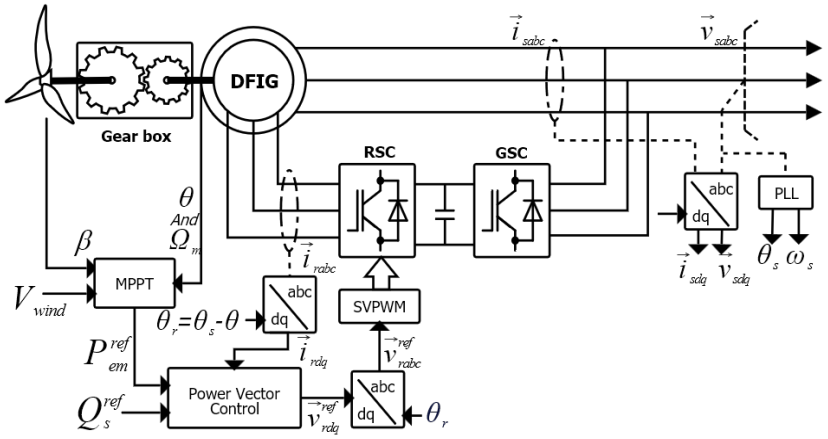


Fig. 1. *Grid connected DFIG system configuration*

2. System modeling

2.1 Aerodynamic model of the WTS

Wind turbines generate electricity using the wind to rotate the blades, which turn a drive shaft connected to a generator. The generator converts this rotational motion into electrical power.

Actuator disk theory provides a simple way to describe how the turbine extracts kinetic energy from the wind, using basic energy balance and Bernoulli's equation. The available wind power is given by Eq. 1.

$$P_{wind} = (\rho A V_{wind}{}^3) / 2 \tag{1}$$

Where A denotes the surface swept by the blades (m^2), and V_{wind} the upwind speed (m/s) and ρ the air density (Kg/m^3).

Although Eq. 1 represents the total wind power accessible at the blades, the power extracted is reduced by the power coefficient Cp, meaning the WTS is able to extract only a portion of this power as shown by Eq. 2 and Eq. 3.

$$C_p = (P_{turbine} / P_{wind}) \tag{2}$$

$$P_{turbine} = C_p . P_{wind} = (C_p . \rho . A . V_{wind}{}^3) / 2 \tag{3}$$

The power factor C_p reflects aerodynamic behavior of a wind turbine system (WTS) and is determined by the turbine's structural characteristics. It is subject to a theoretical upper bound, referred to as the Betz limit, indicating that the analytical highest efficiency for WTSs is 59.3%. In practical, the maximum Cp values for wind turbine rotors typically range from 25% to 45%.

For a given turbine, this coefficient varies with wind velocity, the rotational velocity of the rotor and the blade pitch angle. Accordingly, Cp is commonly formulated as a function of the TSR λ, given in Eq. 4.

$$\lambda = (\Omega_t . R_t / V_{wind}) \tag{4}$$

In this formulation, Ω_t the mechanical velocity of the rotor (rad/s) and R_t refers to the blade length, defined as the distance from the rotor center to the blade tip (m).

Within the framework of the paper, an approximate expression of the power coefficient based on the pitch angle β of the turbine blades and the tip speed ratio λ will be adopted as expressed in Eq. 5.

$$C_p(\lambda,\beta) = (0,5-0,0167.(\beta-2)).\sin((\pi.(\lambda+0,1)) /(18,5-0,3.(\beta-2))) - 0,00184.(\lambda-3).(\beta-2) \quad (5)$$

The characteristics of Cp plotted against λ for multiple pitch angle β values are displayed in Fig .2.

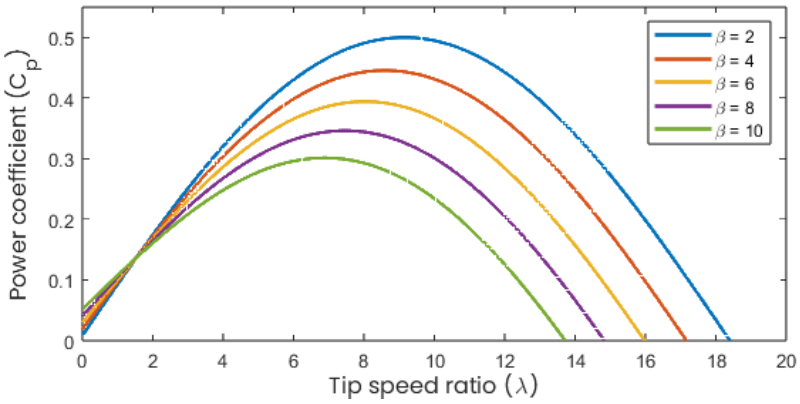


Fig. 2. *Power coefficient Cp variations with respect to λ and β.*

2.2 Doubly fed induction generator model

The DFIG is a wounded rotor asynchronous generator typically modeled under standard assumptions: sinusoidally distributed, symmetrical stator and rotor windings, and no magnetic saturation, core losses, or winding capacitances [8].

A widely used representation is the Park (dq) model, where the dq axes rotate at synchronous speed to simplify analysis. Fig. 3 presents the resulting equivalent circuit in the Park frame, illustrating the stator and rotor windings in a shared coordinate system.

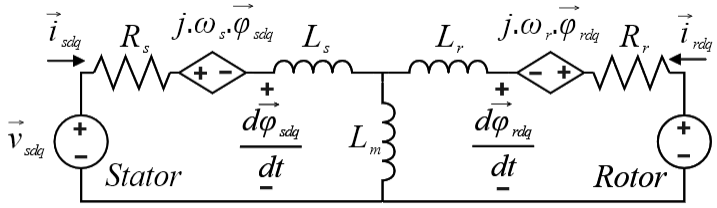


Fig. 3. *Ideal representation of the 3 winding phases (stator, rotor) of the DFIG.*

Within this framework, the stator and rotor quantities dynamics are given by Eq.6, 7, 8, and 9.

$$V_{sd} = R_s.i_{sd} + \left(d\phi_{sd}/dt\right) - \omega_s.\phi_{sq} \quad (6)$$

$$V_{sq} = R_s.i_{sq} + \left(d\phi_{sq}/dt\right) + \omega_s.\phi_{sd} \quad (7)$$

$$V_{rd} = R_r.i_{rd} + \left(d\phi_{rd}/dt\right) - \omega_r.\phi_{rq} \quad (8)$$

$$V_{rq} = R_r.i_{rq} + \left(d\phi_{rq}/dt\right) + \omega_r.\phi_{rd} \quad (9)$$

And the generator flux expressions are expressed by Eq. 10, 11, 12 and 13.

$$\phi_{sd} = L_s.i_{sd} + M_{sr}.i_{rd} \quad (10)$$

$$\phi_{sq} = L_s.i_{sq} + M_{sr}.i_{rq} \quad (11)$$

$$\phi_{rd} = L_r.i_{rd} + M_{sr}.i_{sd} \quad (12)$$

$$\phi_{rq} = L_r.i_{rq} + M_{sr}.i_{sq} \quad (13)$$

Where $L_s = l_s - M_s$ and $L_r = l_r - M_r$ present cyclic inductances. $M_{sr} = 3M_o/2$ is the mutual cyclique inductance. Additionnaly, the angular velocities of the stator and rotor voltages are expressed as $\omega_s = (d\theta_s)/dt$ and $\omega_r = (d\theta_r)/dt$ respectively.

2.3 Power converters model

In DFIG-based wind turbines, the converter is typically an IGBT voltage-source back-to-back unit [10]. It consists of a RSC supplied by the DC bus and a GSC that works as an active rectifier when the machine runs sub-synchronously. The GSC is then wired to the three-phase grid through a filtering inductor, as shown in Fig. 4.

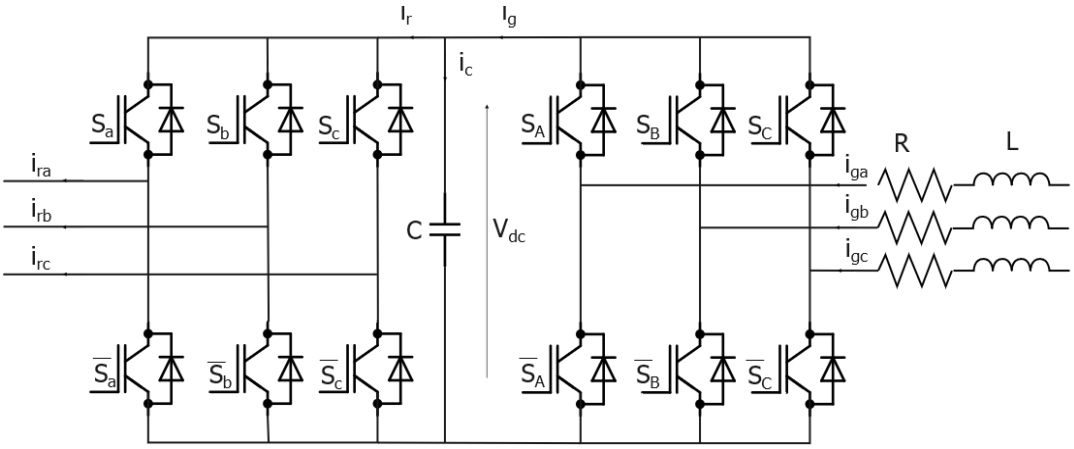


Fig. 4. *Ideal representation of the 3 winding phases (stator, rotor) of the DFIG.*

Assuming a perfect electrical grid and balanced rotor impedance, the following expression can be written as Eq. 14.

$$\begin{pmatrix} V_{ra} \\ V_{rb} \\ V_{rc} \end{pmatrix} = \left(V_{dc}/3\right).\begin{pmatrix} 2 & -1 & -1 \\ -1 & 2 & -1 \\ -1 & -1 & 2 \end{pmatrix}.\begin{pmatrix} S_a \\ S_b \\ S_c \end{pmatrix} \quad (14)$$

3. Control strategy of the WTS

3.1 MPPT biased SMC control strategy

The TSR MPPT method used in this work maximizes energy capture by keeping the fraction of blade tip speed and wind velocity at its optimal operating point. A wind speed sensor provides the actual wind velocity, which allows accurate TSR calculation and ensures the turbine operates at its maximum power coefficient. This sensor-based approach ensures precise tracking of the optimal operating point. Newton's second law for this system is expressed in Eq. (15).

$$\left(d\Omega_m / dt\right) = (Tem - Tm - f.\Omega_m)/J \quad (15)$$

Where Tem the electromagnetic torque supplied by the generator, Tm the mechanical torque applied by the turbine, Ωm is the rotor mechanical speed, f the viscous friction coefficient, and J the moment of inertia. The control scheme model in Fig. 6 is derived.

Materials Research Proceedings 64 (2026) 863-870 https://doi.org/10.21741/9781644904091-107

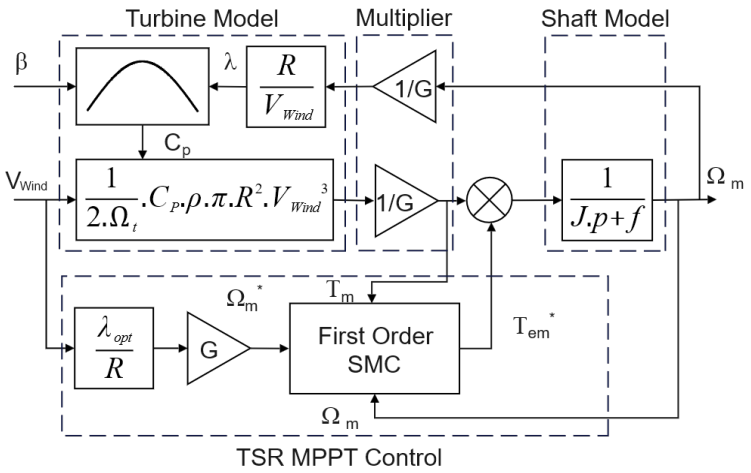


Fig. 6. *Turbine model and TSR-based MPPT control using first order SMC*

The algebraic formula for the mechanical speed control law is given by Eq. 16.

$$T_{em}{}^{*} = K.sign((S(\Omega_m)) + J.\left(d\left(\Omega_m\right)/dt\right) - T_m - f.\Omega_m \tag{16}$$

To overcome the phenomenon of chattering provoked by the sign function of the first order SMC technique, sigmoid functions are proposed, such as the hyperbolic tangent.

3.2 SMC biased FOC of the DFIG

For the DFIG, fluxes are coupled, which results in the coupling of active and reactive power control. The governing equations for this relationship are Eq. 17 and 18.

$$P_s = v_{sd}.i_{sd} + v_{sq}.i_{sq} \tag{17}$$

$$Q_s = v_{sq}.i_{sd} - v_{sd}.i_{sq} \tag{18}$$

To handle this issue, a vector control strategy is used. Previous studies have proposed several approaches [10], including stator-flux-oriented vector control, which aligns the DFIG flux with one axis of the rotating dq frame. Throughout this work, the d-axis is aligned alongside the stator-flux vector. (Fig. 7). Under this condition, the rotor current on the d-axis regulates torque and, consequently, active power, whereas the q-axis current governs reactive power.

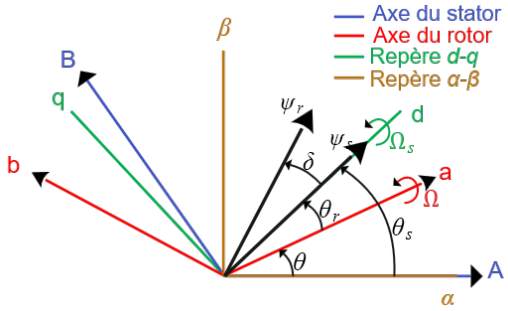


Fig. 7. *Flux vectors and different reference frames*

This technique eliminates the stator flux projection along the q-axis, leading to Eq. 19.

$$\phi_s = \phi_{s_d} \tag{19}$$

Materials Research Proceedings 64 (2026) 863-870 https://doi.org/10.21741/9781644904091-107

As a result, the generator model is simplified to the following set of equations given in Eq. 20 and 21.

$$V_{rd} = R_r.i_{rd} + L_r.\sigma.(di_{rd}/dt) - \omega_r.L_r.i_{rq} \quad (20)$$

$$V_{rq} = R_r.i_{rq} + L_r.\sigma.(di_{rq}/dt) + \omega_r.L_r.i_{rd} + \omega_r.M_{sr}.V_s/(\omega_s.L_s) \quad (21)$$

The formulations of the generator's powers will then be written as in Eq 22 and 23.

$$P_s = -(V_s M_{sr}/L_s).i_{rq} \quad (22)$$

$$Q_s = -(V_s.M_{sr}/L_s).i_{rd} + V_s{}^2/(L_s.\omega_s) \quad (23)$$

It is evident that the both stator powers can be effectively controlled through the regulation of the rotor current. The corresponding block diagram of the simplified generator model operating under the FOC is shown in Fig. 8.

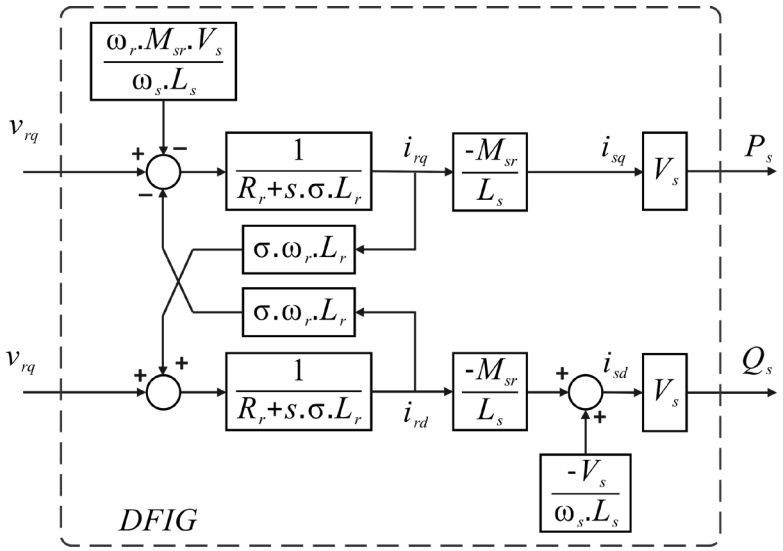


Fig. 8. *Simplified DFIG model with FOC*

Based on the distinct rotor voltage equations, the dynamic state-space model of the rotor currents can be derived as shown in Eq. 24 and 25.

$$\left(di_{rd}/dt\right) = -\left(R_r/\left(L_r.\sigma\right)\right).i_{rd} + \omega_r.i_{rq} + \left(1/\left(L_r.\sigma\right)\right).v_{rd} \quad (24)$$

$$\left(di_{rq}/dt\right) = -\left(R_r/\left(L_r.\sigma\right)\right).i_{rq} - \omega_r.i_{rd} + \left(1/\left(L_r.\sigma\right)\right).v_{rd} - \left(\omega_r.V_s.M_{sr}/\left(\omega_s.L_s.L_r.\sigma\right)\right) \quad (25)$$

It is particularly significant that the resulting system exhibits strong nonlinear behavior, primarily due to the dependency of the direct (d) and quadrature (q) projections of the current available at the rotor, as well as their interaction with the rotational speed of the machine. To control this nonlinear system, a first-order sliding mode control approach is employed. Consequently, the proposed strategy leads to the algebraic expressions given in Eqs. 26 and 27, which define the rotor current control laws.

$$v_{rd} = L_r.\sigma.\dot{i}_{rd}{}^* + R_r.i_{rd} - L_r\sigma.\omega_r.i_{rq} + K.sign(S(i_{rd})) \quad (26)$$

$$v_{rq} = L_r.\sigma.\dot{i}_{rq}{}^* + R_r.i_{rq} + L_r\sigma.\omega_r.i_{rd} + \left(\omega_r.V_s.M_{sr}/\left(\omega_s.L_s\right)\right) + K.sign(S(i_{rq})) \quad (27)$$

Materials Research Proceedings 64 (2026) 863-870 https://doi.org/10.21741/9781644904091-107

4. Results and discussion

This section shows the results of the suggested control strategies, focusing on the TSR-based MPPT using first-order SMC and powers flow control of the DFIG with the same approach. The purpose is to measure the effectiveness of the developed control laws.

To evaluate the SMC-based TSR MPPT approach, a variable wind velocity profile with an average of about 7.5 m/s was used. This profile, shown in Fig. 9(a), reflects realistic wind variations and allows a meaningful test of the controller's robustness and dynamic response.

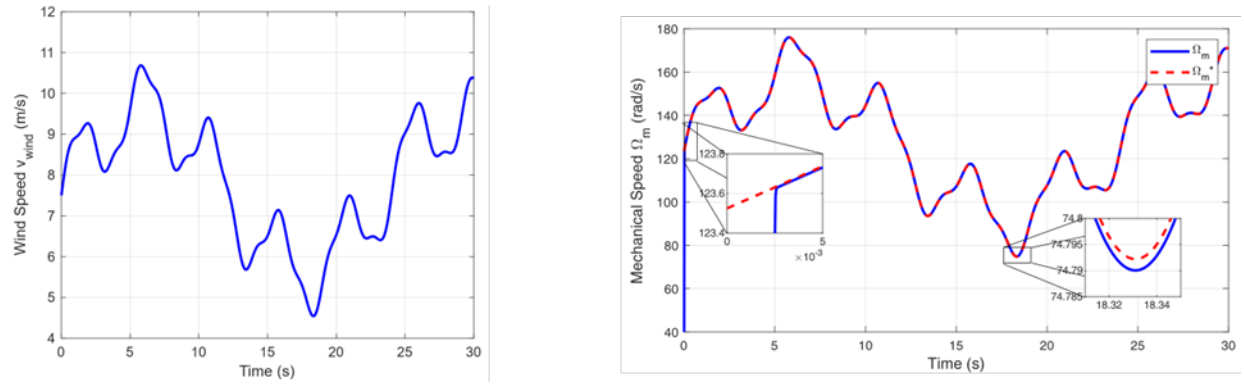


Fig. 9(a). *Wind speed profile over time,* ***(b).*** *Mechanical speed output and mechanical speed reference over time*

The mechanical speed is tracked by the SMC controller with high precision, and a rise time close to 2.5 ms is obtained; even in the presence of sudden wind-speed changes which induce small alterations in both speed and torque commands, tracking error remains minimal, demonstrating excellent robustness as well as fast response (see Fig. 9(b).

Fig. 10 shows that the controller also regulates the generator's powers effectively, achieving a rise time of approximately 1.5 ms. In Fig. 10(a), the active power follows its command closely during both transient and steady-state operation. The reactive power stays near its zero reference with only small deviations as shown in Fig. 10(b).

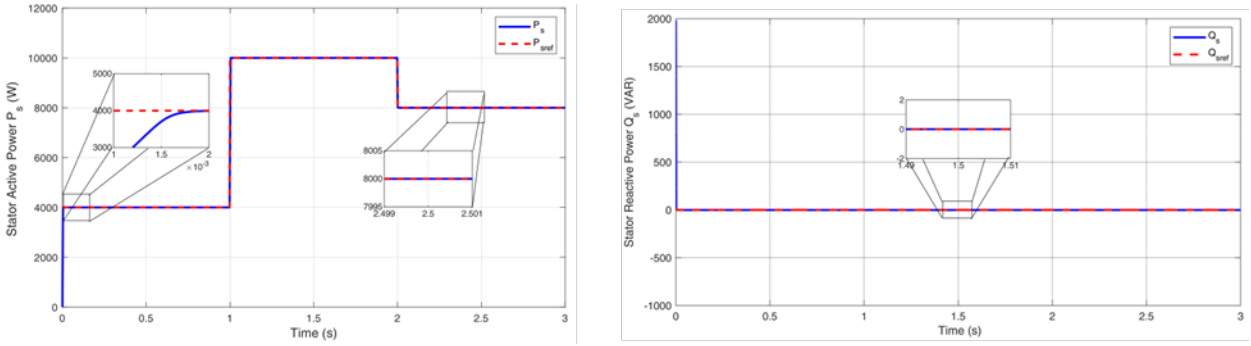


Fig. 10(a). *Stator-side active power output and its command over time,* ***(b).*** *Stator-side reactive power output and its command over time*

The output responses converge precisely to their reference values once transients have settled. Moreover, the system dynamic response is fast, as shown by the rapid convergence in the zoomed-in regions. Another important point is the absence of chattering in the outputs. This comes from using sigmoid functions in the SMC law, which smooth the control action and prevent the high-frequency oscillations seen in conventional SMC. The resulting signals are continuous and smooth, showing better performance and robustness under varying conditions.

5. Conclusion

This paper presented the modeling and control of a DFIG driven WTS. A TSR-based MPPT strategy was combined with a field-oriented control scheme enhanced SMC in order to maximize power extraction and regulate the exchanged active and reactive powers. The overall control architecture was designed to ensure efficient operation and grid compatibility under varying wind conditions.

The simulation findings confirm the performance of the developed control scheme. The SMC-based MPPT achieved accurate speed tracking with a rise time of about 2.5 ms, even during sudden wind variations. In addition, the power control showed a fast response with a rise time of approximately 1.5 ms. Active power closely followed its reference, while reactive power remained near zero. The use of sigmoid functions also eliminated chattering, leading to smooth and stable responses.

However, the study was limited to simulation under ideal conditions. Effects such as parameter uncertainties, grid disturbances, and hardware constraints were not considered. Future work will focus on experimental validation and robustness analysis under more realistic operating conditions.

References

[1] H. Li, Z. Chen, Overview of Wind Turbine Generators, IEEE Trans. Energy Convers (2008).

[2] El Mourabit, Y., Derouich, A., Allouhi, A., El Ghzizal, A., El Ouanjli, N., & Zamzoumyes, O. (2020). Sustainable production of wind energy in the main Morocco's sites using permanent magnet synchronous generators. International Transactions on Electrical Energy Systems, 30(6), e12390. https://doi.org/10.1002/2050-7038.12390

[3] M. Taoussi, M. Karim, B. Bossoufi, Low-speed sensorless control for wind turbine system, WSEAS Trans. Syst. Control, (2017).

[4] S. Karad, R. Thakur, Recent Trends of Control Strategies for Doubly Fed Induction Generator Based Wind Turbine Systems: A Comparative Review, Arch. Comput. Methods Eng (2021).

[5] G. Abad, J. López, M. A. Rodríguez, L. Marroyo, G. Iwanski, Doubly Fed Induction Machine: Modeling and Control for Wind Energy Generation, John Wiley & Sons (2011). https://doi.org/10.1002/9781118104965

[6] E. N. Sanchez, R. Ruiz-Cruz, Doubly Fed Induction Generators: Control for Wind Energy, Automation and Control Engineering Series, CRC Press, Taylor & Francis Group (2015).

[7] D. V. N. Ananth, G. V. Nagesh Kumar, Tip Speed Ratio Based MPPT Algorithm and Improved Field-Oriented Control for Extracting Optimal Real Power and Independent Reactive Power Control for Grid-Connected DFIG, Int. J. Electr. Comput. Eng. (2016). https://doi.org/10.11591/ijece.v6i3.9306

[8] F. Giri (Ed.), AC Electric Motors Control: Advanced Design Techniques and Applications, John Wiley & Sons, 2013. https://doi.org/10.1002/9781118574263